Materials Science & Engineering A 636 (2015) 108–116

Contents lists available at ScienceDirect

Materials Science & Engineering A

journal homepage: www.elsevier.com/locate/msea

# Phase transformation behavior of cold rolled 0.1C–5Mn steel during heating process studied by differential scanning calorimetry

Jun Hu [a,b,*], Wenquan Cao [b], Cunyu Wang [b,c], Han Dong [b], Jian Li [a]

[a] Center for Fuel Cell Innovation, State Key Laboratory of Material Processing and Die & Mould Technology, School of Materials Science and Engineering, Huazhong University of Science and Technology, Wuhan 430074, China
[b] Special Steel Institute, Central Iron and Steel Research Institute, No. 76 XueYuanNanLu, Beijing 100081, China
[c] Taiyuan Iron and Steel (group) Co Ltd., Taiyuan 030003, China

ARTICLE INFO

*Article history:*
Received 4 February 2015
Received in revised form
18 March 2015
Accepted 20 March 2015
Available online 31 March 2015

*Keywords:*
Differential Scanning Calorimetry (DSC)
$\alpha \rightarrow \gamma$ transformation
Activation energy
Stored energy
Mechanical property

ABSTRACT

The microstructural evolution of a cold-rolled steel 0.1C–5Mn was characterized by SEM and EBSD, and the $\alpha \rightarrow \gamma$ phase transformation of the steel was determined by differential scanning calorimetry (DSC) upon heating. The retained austenite fraction and the dislocation density were examined by XRD. Based on the DSC data, the Kissinger's method was used to calculate the activation energy of the cold rolled steel. The activation energy of 363–824 kJ/mol suggested a sluggish phase transformation during the heating process and it showed an increase trend with the increase of thickness reduction which was affected by the density of the dislocation and the drag effect by the solute Mn. The stored energy (14–30 J/g) was associated with energy released from the $\alpha \rightarrow \gamma$ transformation during the heating process. Based on the effects of temperature on the phase transformation behavior, the cold rolled medium-Mn steel with different thickness reductions were annealed at the onset phase transformation temperature with 5 min and 6 h, which results in a very good combination strength and ductility.



## 1. Introduction

In recent years, increasing attention has been given to the development of high strength steels for automobile body panels. The general requirement is that these steels are strong and ductile to meet upgraded safety standards in automotive industries so that the vehicles made from these steels have good worthiness after crashing. At the same time, high strength steels can reduce the total weight of the vehicles to improve the fuel economy and to protect environment due to reduced $CO_2$ emission. Therefore, steels with a good combination of high strength and high ductility have been studied worldwide [1,2].

As a typical representative of the third generation of automotive steel, the medium Mn steel is supposed to be a very promising material to produce automotive steel sheets with high strength and high ductility [3–5]. It was reported that the unique mechanical properties of the medium Mn steel was related to a high volume fraction of retained austenite phase produced by a heat treatment process for the forging state [6]. Therefore the heat treatment process has an important effect on the volume of the retained austenite and consequently the final mechanical properties of the medium Mn steel. A key issue of the heat treatment is how to formulate the heat treatment process.

High strength automotive steels are usually applied in cold rolled and annealed state. The hot rolled steels are further cold rolled followed by soft-annealing. Finally the annealing is processed for application. Although the annealing behaviors of the hot rolled medium-Mn steel have been studied extensively, the annealing behaviors of the cold rolled medium-Mn steels were less investigated. In order to produce cold rolled sheet steel, hot rolled medium-Mn steel has to be soft annealed and then cold rolled into different strains. The cold deformation would introduce high density dislocations and dislocation boundaries in deformation microstructures. During subsequent annealing, recovery and/or recrystallization occur in the steel. Phase transformation of the cold rolled ferrite into austenite would also take place. Thus a systematic study of the annealing and phase transformation of the cold rolled medium-Mn steel is crucial to the fabrication of the third generation automobile sheet steel with high strength and high ductility. During deformation, stored energy is increased due to the creation of dislocations and boundaries in the deformed microstructure. The stored energy could be released by recovery, recrystallization and phase transformation, which is usually measured by differential scanning calorimetry (DSC) [7,8]. The DSC measurement can not only reflect the cold deformation process, but also build experimental and theoretical basis for the controlling of cold rolling and

* Corresponding author at: Center for Fuel Cell Innovation, State Key Laboratory of Material Processing and Die & Mould Technology, School of Materials Science and Engineering, Huazhong University of Science and Technology, Wuhan 430074, China. Tel.: +86 18627011247.
*E-mail address:* hujun-jay2004@163.com (J. Hu).

http://dx.doi.org/10.1016/j.msea.2015.03.080
0921-5093/

the determination of annealing parameters of the cold rolled medium-Mn steel.

In this paper, the annealing behaviors of the cold rolled medium-Mn steel with different thickness reductions were studied by DSC, scanning electron microscopy (SEM), electron back scattered diffraction (EBSD) and X-rays diffractions (XRD). The objective of this study is to investigate the $\alpha \rightarrow \gamma$ transformation of the cold rolled steel during the annealing process. What is more, the annealing of the cold rolled medium-Mn steel was properly controlled by choosing the onset temperature of annealing measured by DSC to verify the possibility to produce a steel with high strength and high ductility.

## 2. Experiments and methods of analysis

### 2.1. Materials and Processing

The chemical composition of the steel in the present experiment was shown in Table 1. The steel was smelted in 50 kg vacuum induction furnace and casted into an ingot. The ingot was first forged into a 30 mm thick square slab followed by homogenization at 1200 °C for 2 h. Then the slab was hot rolled in the temperature range of 1200–900 °C to a thin slab with 4 mm thickness followed by air cooling to room temperature. The hot rolled sheet was further annealed at 650 °C with 6 h (soft annealing) resulting in a ferrite and austenite duplex structure. Finally the soft annealed steel was cold rolled into different reductions from 5% to 80% as shown in Table 2. The cold-rolled steel was finally annealed at 650 °C for 5 min and 6 h, and the steel of 50% reduction was annealed at 625 °C for 5 min and 6 h additionally.

### 2.2. Differential scanning calorimetry (DSC)

DSC samples having 5 mm in diameter were punched, ground and cleaned from the cold rolled sheet. The samples were measured in a TA Instruments Q100 heat-flux typed DSC with the TZero™ sensor [9]. During DSC measurement, the samples were placed in alumina pans and protected by a high purity nitrogen atmosphere with a gas flow speed of $\sim$50 ml min$^{-1}$. Standard In, Zn and Al samples were used for heat flow and temperature measurement calibration at all heating rates to ensure the accuracy of measurements. For thermodynamic studies, samples were heated from room temperature to 900 °C by three different rates (10, 25 and 50 K/min, respectively), hold for 10 min and cooled to room temperature in air. Two samples were examined for each heating rate. Stored energies were calculated by integrating the areas under the corresponding peaks subtracted by the base line between the onset and finish temperatures. Based on the DSC measurements of different heating rates, the activation energy of the test material was calculated by Kissinger's method.

### 2.3. Microstructural analysis

The microstructure in the transverse section of cold rolled steel was examined by SEM using a S-4300 and the microstructure in the rolling plane was characterized by EBSD equipped in a LEO 1530 thermal field emission gun SEM. The EBSD maps were post-processed by reducing all the single pixels, which were considered to be the wrong indexed results. In order to avoid the disturbance of the noise, only the grain boundaries with misorientation angle more than 2° were illustrated in the EBSD maps. The volume fraction of residual austenite and dislocation densities on the rolling surface after grinding and polishing were determined by XRD in a PHILIPS APD-10 X-ray diffractometer. For XRD measurement, the samples were mechanical polished followed by electrolyzing at 5 V for 50 s in a 10% chromic acid electrolyte to remove the surface stress. The XRD was installed with a Co target and a graphite crystal monochromator, and was operated with a tube current of 30 mA and a voltage of 30 kV. Diffraction patterns were obtained by step scan mode. Scanning angle $2\theta$ ranged from 45° to 115°; the scanning step was 0.02° and integration time 0.4 s. The volume fraction of retained austenite was calculated by the integral intensities of ferrite (200) and (211) and austenitic (200), (220) and (311) peaks by the following equation [10]:

$$V_i = \frac{1}{1+G(I_\alpha/I_\gamma)} \quad (1)$$

where $V_i$ is the volume fraction of retained austenite; $G$ is the parameter of crystal surface in austenite and martensite; $I_\alpha$ and $I_\gamma$ are the integral intensities of the peaks in martensite and austenite, respectively.

**Table 1**
Chemical composition of the tested alloy (wt%).

| C | Mn | P | S | N |
|---|---|---|---|---|
| 0.1 | 5 | 0.008 | 0.002 | 30 ppm |

**Table 2**
The thickness of the cold-rolled sheet with different reduction (mm).

| Reduction (%) | 0 | 5 | 10 | 30 | 50 | 70 | 80 |
|---|---|---|---|---|---|---|---|
| Thickness | 4.0 | 3.8 | 3.6 | 2.8 | 2.0 | 1.2 | 0.8 |

### 2.4. Tensile test

Mechanical properties of the steel after annealing were measured by tensile test to evaluate the $\alpha \rightarrow \gamma$ transformation behavior of the annealed materials. After annealing the steels were machined into a tensile specimen according to the standard geometry of the tensile specimen (GB/T 228.1–2010). The uniaxial tensile test was carried out with a strain rate of $2.5 \times 10^{-4}$/s on the WE300B tensile testing machine.

## 3. Results

### 3.1. Microstructure of the cold rolled steel examined by SEM and EBSD

The microstructural evolution of 0.1C–5Mn steel cold rolled to reduction of 10%, 30%, 50% and 70% was examined in transverse section and was shown in Fig. 1. Before cold rolling, the steel was soft annealed at 650 °C for 6 h. So the microstructure is composed of duplex-phase of austenite and ferrite with lamellar shaped grains [11]. With the increasing of the cold rolling reduction, the grains are elongated along the rolling direction during the cold rolling process. At low strains (e.g. 10%), the microstructure is similar to that before cold rolling. Beside the duplex phases there are some precipitates in the microstructure. After rolled to medium strains (e.g. 50%), a lamellar deformation microstructure lying approximately parallel to the rolling plane develops (Fig. 1c). The stretch clearly shows that the elongated structure has a preferred orientation with a certain degree. After rolled to high strains (e.g. 70%), the grains were further refined and distorted resulting in a fiber microstructure.

The EBSD maps of the cold rolled steel measured in the rolling plane was used to show the evolutions of microstructure, phase transformation and the boundary characters in Fig. 2. Two main features can be seen from the figure. One is the disappearing of

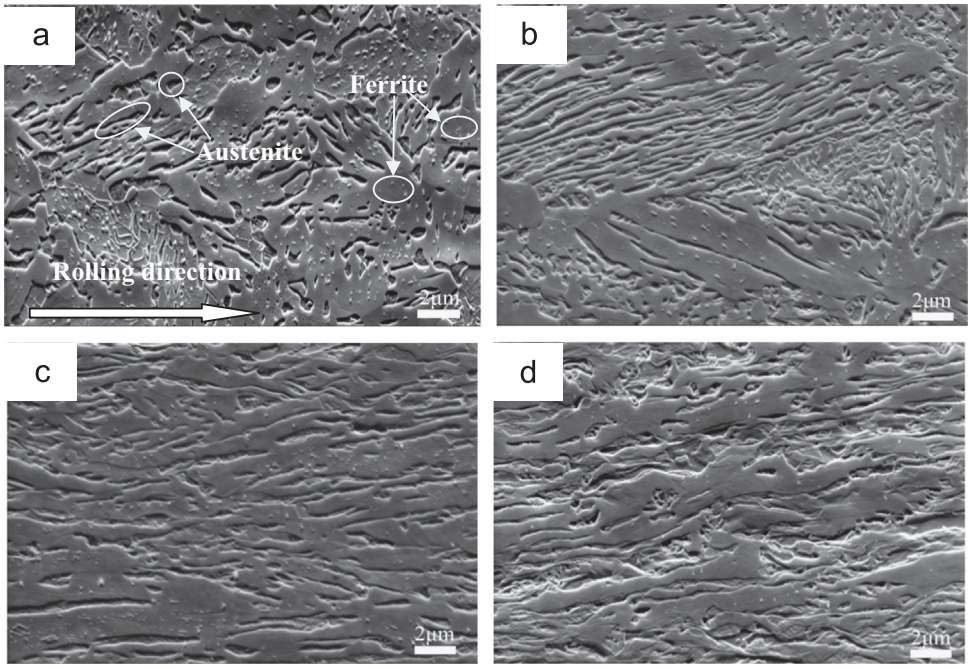


**Fig. 1.** SEM micrographs of the steel after cold rolled to (a) 10%, (b) 30%, (c) 50% and (d) 70% reductions in thickness, respectively.

austenite with increasing rolling reductions. After 5% strain as seen in Fig. 2a, most of the austenite could be clearly seen. When the steel was deformed to 10%, the volume fraction of austenite was reduced, as shown in Fig. 2b. After rolling strain increasing to 30% and 50%, no austenite can be detected in the microstructure, as shown in Fig. 2c and d. The deceasing of the austenite volume fraction implies that phase transformation from austenite to martensite takes place during the rolling process. The second feature is the changing of grain shapes and the increasing of high angle boundaries. After deformed to low stains (Fig. 2a and b) the main microstructural feature is the elongated grains with high angle grain boundaries and low angle subgrain boundaries. However, with the strain increasing up to 30% and 50%, no elongated grain can be seen and most of the grains are nearly granular surrounded by high angle grain boundaries (Fig. 2c and d). In addition, many high angle boundaries are developed after deformation.

### 3.2. Volume fraction of austenite and dislocation density

The volume fraction of austenite and the density of dislocation during cold rolling are shown in Fig. 3a and b, respectively. It is seen that the volume fraction of retained austenite is about 18% before cold rolling. The volume is reduced to 12% and 9% after deformed to 5% and 10% reduction in thickness, respectively. It continuously decreases to about 2% after 30% reduction in thickness. Then the volume fraction has little change with future increasing of rolling reductions. Meanwhile the dislocation density increases approximately linearly with the rolling reduction. Comparing with the evolution of volume fraction of austenite during deformation, it can be deduced that the increasing of the dislocation density in the cold rolled state are caused by deformation of ferrite and not by the phase transformation of austenite. The reason could be the dislocation proliferation mechanism during the cold rolling process.

### 3.3. DSC scanning heat flow curves

Fig. 4 shows the curves of heat flow versus temperature of cold rolled samples measured at different heating rates. It can be seen that there are two endothermic peaks in all DSC curves with different heating rates. According to Ref. [12], the second peak is corresponded to the $\alpha \rightarrow \gamma$ transformation, including the nucleation and growth of the austenite. So this peak was studied and the stored energy was calculated in this paper.

The onset, peak and finish temperatures for the phase transformation are represented in Fig. 5a. It can be seen that the onset temperatures for the phase transformation are in the range between 550 °C and 680 °C, the peak temperatures 750 and 780 °C and the finish temperatures 800 and 850 °C. All other temperatures are shifted to higher values with increasing heating rates excepted the onset temperature of the samples cold rolled to 70% and 80% and with a heating rate of 10 K/min. The shift of temperatures to higher values means that the phase transformation is not only time dependent but temperature dependent. It should be also noticed that the onset temperature of the 50% rolled steel is the lowest among all samples. The stored energy at different heating rates and the average stored energy are shown in Fig. 5b. It can be seen that the stored energies have little variations at different hearing rates. While, the average stored energy first drops slightly before cold rolled to 10%. Then it quickly increases with deformation strains and reaches the maximum value of about 30 J/g at 50% thickness reduction. With future increasing the deformation strain, the average stored energy decreases again. Therefore the stored energies are not affected significantly by the heating rate but are strongly dependent on the deformation strain. It is also interesting to found that the average stored energy has an opposite trend versus the deformation strain to the onset temperature of the phase transformation. Both the maximum of the stored energy and the lowest onset temperature occur in the sample cold rolled to 50%.

The onset temperature, peak temperature and finish temperature are very useful to determine the heat treatment parameters of

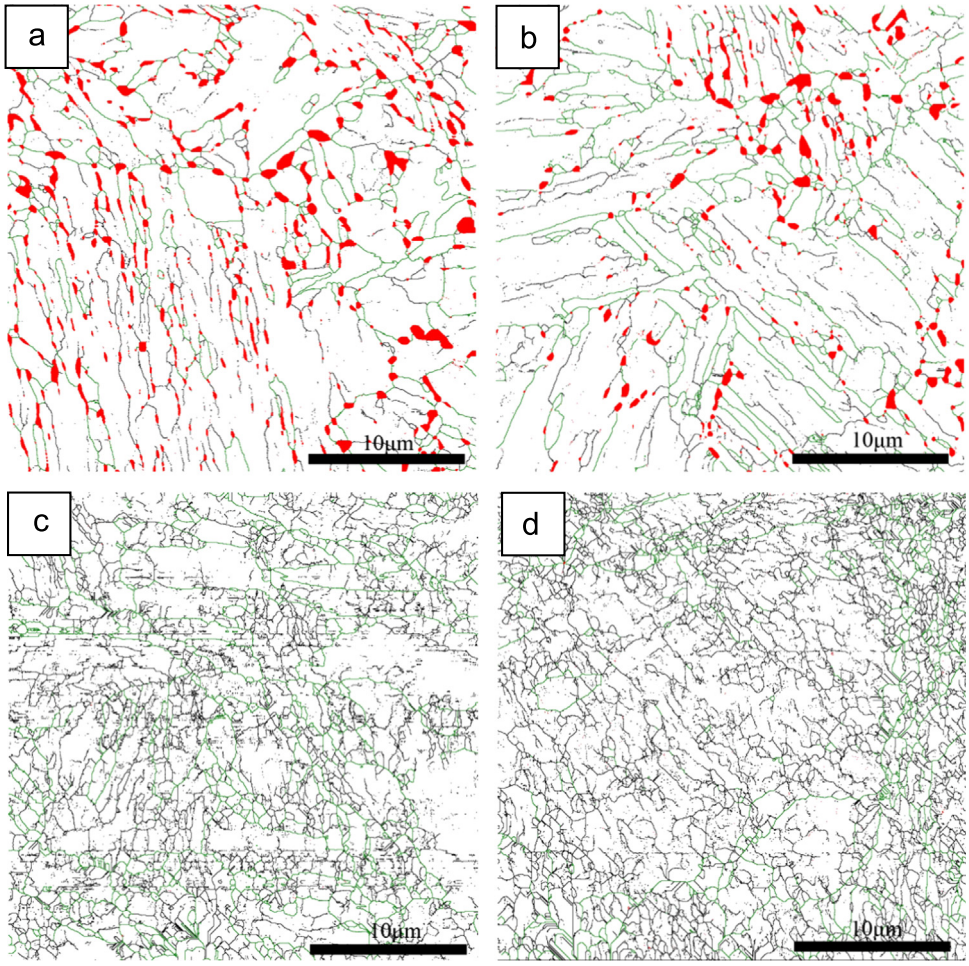


**Fig. 2.** EBSD maps of the steel after cold rolling (a) 5%, (b) 10%, (c) 30% and (d) 50%, respectively. In the maps low-angle boundaries ($2^\circ \le \theta \le 15^\circ$) and high-angle boundaries ($\theta > 15^\circ$) are depicted by green lines and black lines, respectively. The red color represents the austenite phase. (For interpretation of the references to color in this figure legend, the reader is referred to the web version of this article.)

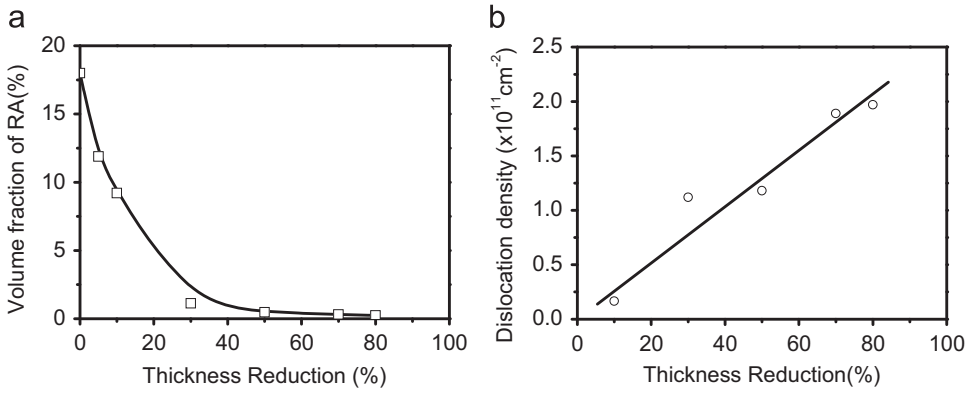


**Fig. 3.** (a) The volume fraction of retained austenite and (b) dislocation density of the cold rolled medium-Mn steel as a function of rolling reduction in thickness.

the annealing process. It has been well discussed that most of cold rolled ferrite phase will transform into austenite if a sample is annealed above the peak temperature [13]. Thus, the austenite is unstable and will transform to martensite during air cooling to room temperature. Therefore the annealing of the cold rolled steel should be conducted at the onset temperature to ensure a certain amount of carbon-enriched austenite retained during the annealing process.

### 3.4. Activation energy of phase transformation

The activation energy of the steel during the $\alpha \rightarrow \gamma$ phase transformation was calculated by Kissinger's method [14] as following,

$$\ln\left(\beta/T_P^2\right) = -\Delta G/RT_P + C \quad (2)$$

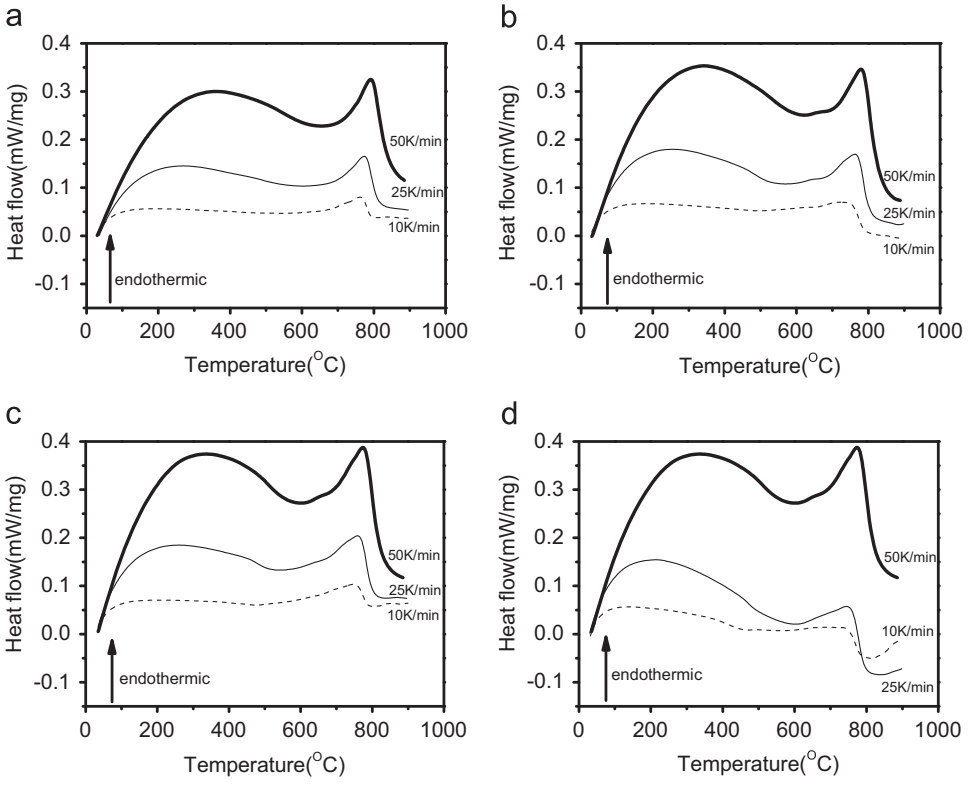


**Fig. 4.** Curves of heat flow versus temperature of (a) 5%, (b) 30%, (c) 50% and (d) 70% cold rolled samples measured at different heating rates (K/min).

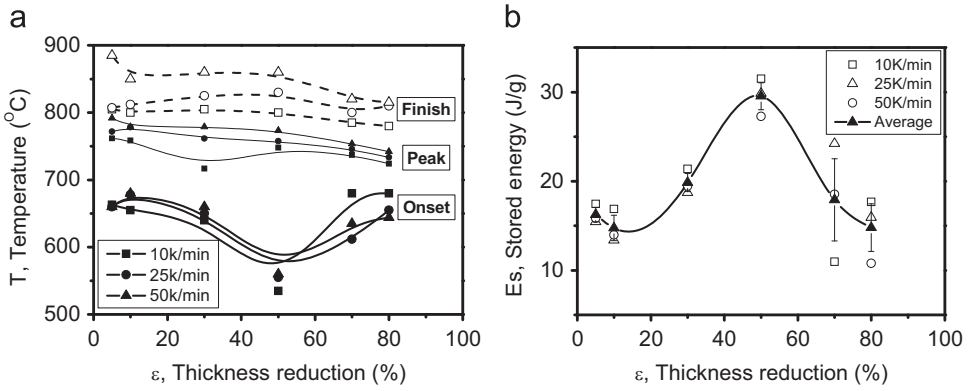


**Fig. 5.** (a) Phase transformation temperature and (b) stored energy as a function of deformation strain at different heating rates.

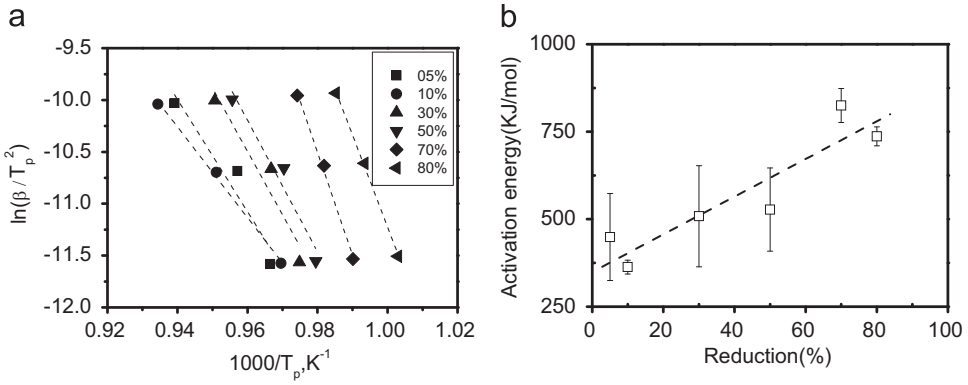


**Fig. 6.** (a) Plots of $\ln\left(\beta/T_P^2\right) - 1000/T_p$ of the cold rolled samples during the annealing process; and (b) the activation energy as a function of deformation strain.

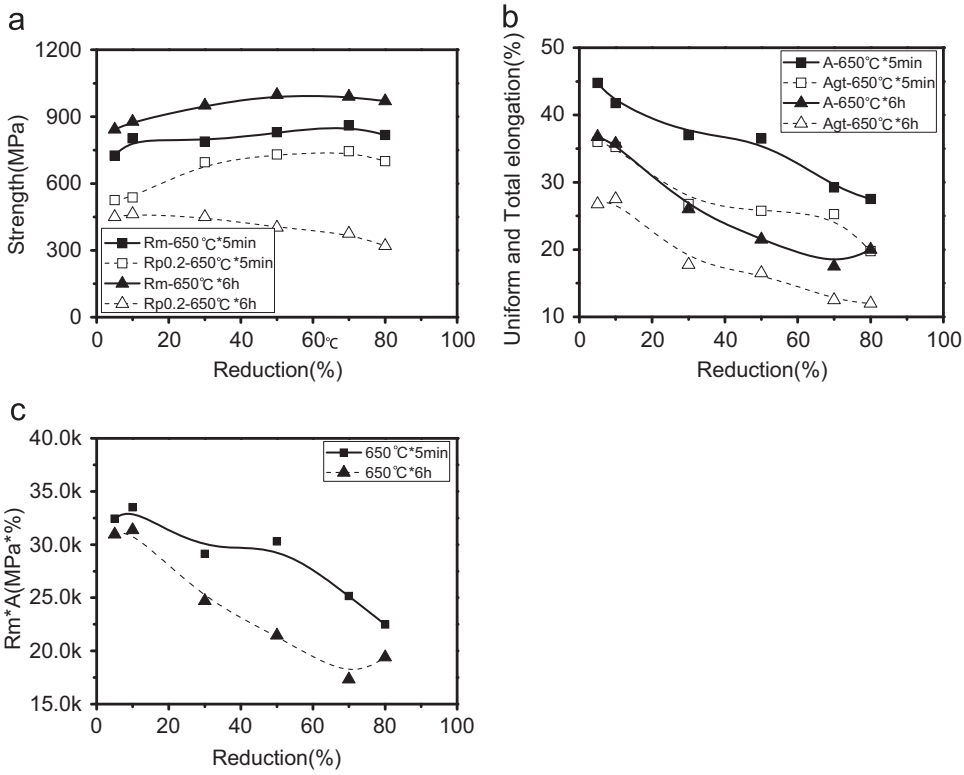


**Fig. 7.** Plots of (a) Rm and Rp0.2, (b) *A* and Agt, and (c) Rm*A as a function of deformation strain of the medium Mn steel after cold rolled and annealing processing.

**Table 3**
The mechanical properties of the 50% reduction steel after different annealing processes.

| Process | Rm [MPa] | Rp0.2 [MPa] | *A* [%] | Agt [%] | Rm∗*A* [GPa%] |
|---|---|---|---|---|---|
| 625 °C × 5 min | 817 | 815.5 | 23.75 | 11.00 | 19.4 |
| 625 °C × 6 h | 722 | 641 | 47.75 | 35.50 | 34.5 |
| 650 °C × 5 min | 830 | 730 | 36.50 | 25.75 | 30.3 |
| 650 °C × 6 h | 997.5 | 402.5 | 21.50 | 16.50 | 21.4 |

where $\beta$ is the heating rate in the DSC test, $T_P$ the peak temperature of the phase transformation in Kelvin, $R$ the universal gas content (8.314 J $K^{-1}$ $mol^{-1}$), $\Delta G$ the activation energy and $C$ a constant. When $\ln\left(\beta/T_P^2\right)$ is plotted against $1/T_P$, the slope of the linear fit is usually applied to calculate the activation energy of $\Delta G$.

Fig. 6a is the plot of $\ln\left(\beta/T_P^2\right) - 1000/T_P$ of the samples cold rolled different strains during the annealing process. The activation energies of these samples estimated by linear fitting from the plots in Fig. 6a are shown in Fig. 6b. It is seen that the activation energies of the cold rolled steel range between 363 and 824 kJ/mol, increasing with the deformation strain with large scatters.

### 3.5. Annealing parameters design and mechanical properties

As it is shown that the onset temperatures range from 550 to 680 °C, the annealing temperature of the present cold rolled medium-Mn steel is set to be 650 °C. So all the cold rolled samples were annealed at 650 °C with 5 min and 6 h respectively and the steel of 50% reduction was annealed at 625 °C with 5 min and 6 h additionally to produce a series of high strength and high ductility steels. The mechanical properties of these steels were tested and are shown in Fig. 7. As seen in Fig. 7a, the tensile strength (Rm) and yield strength (Rp0.2, measured at 0.2% offset) increase gradually with the strain and they both drop slightly at the strain of 80% for the steel annealed at 650 °C for 5 min. While, the Rm increases and the Rp0.2 decreases gradually with the strain for the steel annealed at 650 °C for 6 h. Compared with the steel annealed for 5 min, the 6 h annealed steel have larger Rm and smaller Rp0.2. The uniform elongation (Agt) and total elongation (*A*) both decrease with the deformation strain in the 5 min and 6 h annealed steels, and both Agt and *A* are much greater in the 5 min annealed steels than those in the 6 h annealed steels, as shown in Fig. 7b.

Fig. 7c shows the product of tensile strength to total elongation (Rm*A) of the steels after different rolling and annealing processings. The product Rm*A, which can indicate the forming ability and the deformation energy absorbed during collision, is applied to evaluate the combined mechanical properties of the present medium-Mn steels. It can be seen that the product decreases rapidly when the strain is larger than 10% for the 6 h annealed steels although it has a small raise at 80% reduction. However, for the 5 min annealed steels, two local maxima (33.5 GPa% and 30.3 GPa%, respectively) are observed, corresponding to reductions of 10% and 50%, respectively. The values of Rm∗*A* of the 6 h annealed steels are smaller than those of the 5 min annealed steels. This means that long time annealing at 650 °C is not benefit for the production of high strength and high ductility steels. Further study is necessary to discuss the possibility of annealing at relative high temperatures.

And the mechanical properties of the 50% reduction steel after different annealings were shown in Table 3. It can be seen that the mechanical properties were even better of the 50% reduction steel annealing at 625 °C for 6 h than annealing at 650 °C for 5 min. The product of Rm and *A* was 34.5 GPa% which revealed excellent mechanical properties.

## 4. Discussions

### 4.1. Activation energy of phase transformation

The DSC curves depict two broad endothermic peaks corresponding to temperature ranges of 200–400 °C and 600–800 °C, as shown in Fig. 4. It was supposed that the recovery and/or recrystallization take place prior to the phase transformation in the temperature range of 200–400 °C, as reported by Scholz et al. [15]. However, the combined energies released in the peaks approximately equals to 19 J/mol, which are much lower than the value of the stored energy (14.8 J/g ≈ 830 J/mol) of the present steel at 80% reduction. So the peaks in the temperature range of 200–400 °C in the present DSC curves are believed corresponding to the recovery and/or recrystallization. While the second peak in the temperature range 600–800 °C is related to phase transformation. The activation energy of phase transformation was then calculated by using the second peaks.

As shown in Fig. 6b, the activation energies of the cold rolled medium-Mn steel range between 363 and 824 kJ/mol. These values are much higher than that of self-diffusion of Fe (251–282 kJ/mol) [16]. It is well known that the activation energy measured by DSC includes not only the activation energy of austenite nucleation but also the activation energy of the austenite growth. Thus it is reasonable that the activation energy calculated from DSC is larger than that of the self-diffusion energy. It is also shown in Fig. 6b that the calculated activation energy is strongly affected by the reduction of cold rolling, being approximately linearly proportional to the reduction. This increasing of the activation energy could be related to the existence of austenite in the deformation microstructure. In the low strain deformed steel, the retained austenite could be regarded as the nucleation site and thus the total activation energy calculated from DSC is mainly contributed from the self-diffusion energy of Fe-atom and Mn-atom. However, with increasing rolling reduction, most of the austenite was transformed into martensite. Thus, the activation energy measured from DSC is not only controlled by austenite nucleation but also austenite growth. Therefore the activation energy increases with increasing rolling reduction, as shown in Fig. 6b.

### 4.2. Apparent stored energy measured by DSC

The apparent stored energy of the medium-Mn steel firstly increases then decreases with rolling reduction, as shown in Fig. 5b. The lowest value of stored energy is about 15 J/g when the rolling reductions in thickness are lower than 20% and larger than 70%. The maximum value is about 30 J/g at 50% reduction thickness. Compared with the results in literatures as given in Table 4, the apparent stored energies of the medium-Mn steel after different thickness reductions are relative large. The apparent stored energy after conventional cold rolling is normally less than 10 J/g in literatures, which is significantly smaller than the maximum stored energy of present medium-Mn steel. Therefore the energy release mechanism of the present rolled medium-Mn steel might be different to that in literatures.

As reported in Refs. [15,17,18], the stored energy is mainly caused by the deformation induced structures. However, the apparent stored energy is not only caused by the structure energy but also the phase transformation in the present experiment. The total stored energy of conventional cold working is assumed to comprise the additive contributions from statistically stored/loose dislocations in the bulk, geometrically necessary dislocations at subgrain/grain boundaries, internal stresses and point defects [19]. The energy from the subgrain boundaries ($E_b$), the energy from point defects ($E_v$), mainly in the form of vacancies and the energy from dislocation ($E_d$) were obtained referring to Ref. [19]. It is found that $E_b$ is less than 1 J/g, $E_v$ about 1–2 J/g and $E_d$ also less than 1 J/g. Putting all these energies together, the value is about 5 J/g at most, which is significantly lower than the measured stored energy by DSC in this study.

**Table 4**
The stored energy values of various irons and steels compiled from the literature.

| Processing | Material | Stored energy $E_s$ (J/g) | References |
|---|---|---|---|
| 80% cold rolled | 99.999% Fe | 0.39 | [15] |
| 85% cold rolled | High-purity Iron | 6.3 | [17] |
| 80% cold rolled | Fe–0.015%Nb | 0.87 | [18] |

As mentioned in Section 3, phase transformation from ferrite to austenite takes place in the cold rolled medium-Mn steel. Thus contribution of phase transformation to the measured energy should be considered. It has been reported that high concentrations of ~9% Mn and ~0.5% C could be more easily reached on the boundary and the segregations of Mn and C onto the boundaries can account for the nucleation of the austenite phase and the growth of the austenite which are constrained by the diffusion of Mn onto the boundaries [20]. In order to demonstrate this Gibbs free energy difference, the Thermo-CALC commercial software package was used to calculate the Gibbs free energy of both ferrite and austenite at different temperatures as listed in Table 5. It is found that the $\Delta G$ decreases from 2700 J/mol (50 J/g) to 850 J/mol (15.8 J/g) at the temperature range 450–750 °C. It was also pointed out in Section 3.3 that both the maximum stored energy and the onset temperature are found in the steel after 50% reduction. Thus it is interesting to build the relationship between the onset temperature and the stored energy, which was shown in Fig. 8a. It can be seen that a very good inverse linear relationship could be found between the apparent stored energy and the onset temperature, which indicates that the onset temperature of phase transformation might be determined by the apparent stored energy in the medium-Mn steel. Fig. 8b shows the measured stored energy (Es) and the difference of Gibbs free energy between $\alpha$ and $\gamma$ at the onset temperature ($\Delta G$), in which a very good linear relationship can be seen. This indicates that the apparent stored energy is mainly contributed from the phase transformation. It also should be noticed that the Es is slightly lower than the $\Delta G$, which could be interpreted by the increased temperature of the phase transformation during DSC measurement.

### 4.3. Mechanical properties

Based on the onset temperature measured by DSC, the annealing temperature was chosen. It was found that the product of Rm and $A$ slightly decreases with increasing reduction of thickness when the sample was annealed at 650 °C for 5 min. However, Rm*$A$ decreases quickly with thickness reduction when it was annealed at 650 °C for 6 h. The longer the annealing time, the larger volume fraction of austenite will be developed after annealing as shown in Fig. 9a. It is noteworthy that both the uniform elongation of the steels for different annealing time increases with the austenite volume fraction approximately linearly but it was higher for a short time annealing as shown in Fig. 9b. It is known that the uniform elongation is related to not only the amount and stability of the retained austenite but also the austenite and ferrite grain size in the steel. It has been proved that both the austenite and ferrite grain size is smaller than 0.4 μm in the 1 min annealed state but coarsens to approx. 1 μm after 6 h annealing at 650 °C for the cold rolled steel [20].

Corresponding to the results as shown in Fig. 5a, the onset temperature was the lowest for the 50% reduction and then the steel was annealed at 625 °C. It revealed better mechanical properties for the steel annealed for 6 h at 625 °C than annealed

**Table 5**
The calculated Gibbs free energy of $\alpha \rightarrow \gamma$ transformation ($\Delta G_{\alpha\rightarrow\gamma}$) along the temperature.

| G (J/mol) | 450 | 500 | 550 | 600 | 650 | 700 | 750 |
|---|---|---|---|---|---|---|---|
| $G_\gamma$ | −2.925*E*4 | −3.181*E*4 | −3.452*E*4 | −3.708*E*4 | −3.964*E*4 | −4.263*E*4 | −4.562*E*4 |
| $G_\alpha$ | −2.655*E*4 | −2.925*E*4 | −3.210*E*4 | −3.509*E*4 | −3.822*E*4 | −4.135*E*4 | −4.477*E*4 |
| $\Delta G$ | −2700 | −2560 | −2420 | −1990 | −1420 | −1280 | −850 |

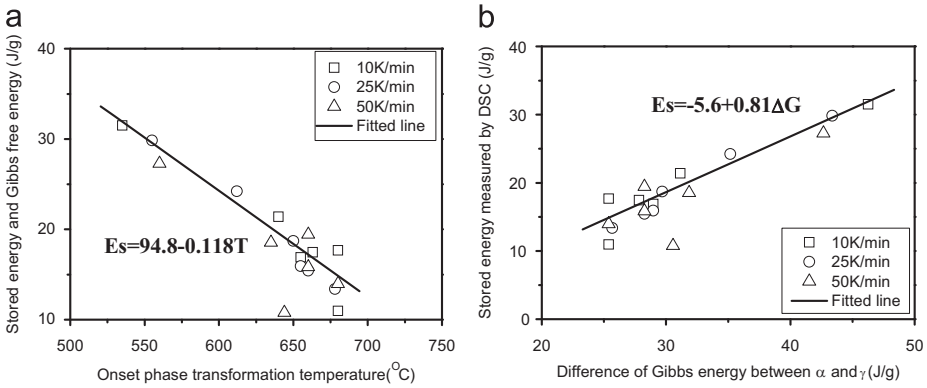


**Fig. 8.** (a) Stored energy as a function of the onset phase transformation temperature, and (b) stored energy as a function of the difference of the Gibbs energy between ferrite and the austenite.

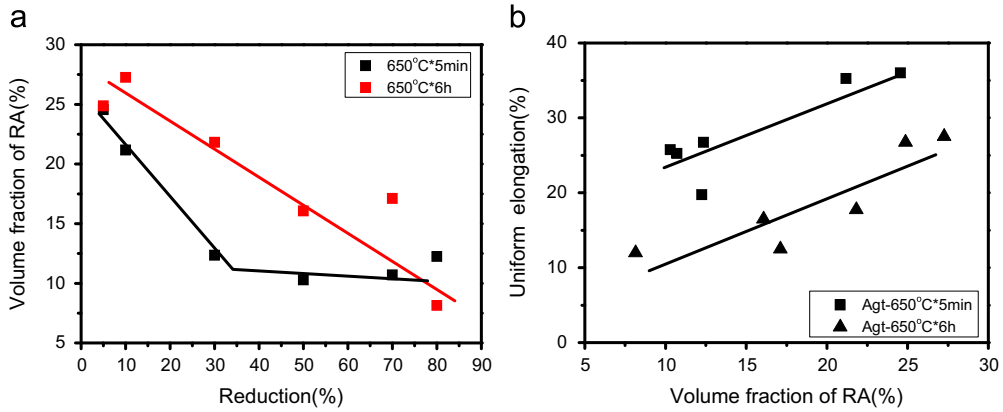


**Fig. 9.** (a) The volume fraction of retained austenite in the steel after annealing and (b) relationship between uniform elongation and the austenite volume fraction.

for 5 min at 650 °C. But it was not so good for 5 min annealing at 625 °C. It may be explained that short time annealing is not enough to develop sufficient austenite in the steel at 625 °C and it will develop large volume fraction of austenite with high mechanical stability so that it will obtain good mechanical properties.

For the present steel, the product of Rm and *A* larger than 30 GPa% can be obtained when the rolling reduction is lower than 50% and the material was annealed at 650 °C for 5 min. However, Rm*A* larger than 30 GPa% can only be obtained after annealing at 650 °C for 6 h when the rolling reduction is lower than 20%. Therefore, the steel with thickness reduction less than 50% is suitable for short time annealing, such as continuous annealing (CA) in industrial manufacture, while the steel with thickness reduction less than 20% is suitable for long time annealing, such as batch annealing (BA). Further thorough study is necessary to reveal the annealing temperature and time effects on the mechanical property of the study of medium-Mn steel.

## 5. Conclusions

The annealing behaviors of the cold rolled medium-Mn steel were studied in this study to explore the ferrite to austenite transformation behavior. The microstructure, stored energy and the activation energy were examined and discussed. Conclusions were drawn as follows:

(1) The variation of the activation energy (from 363 to 824 kJ/mol) suggests a sluggish phase transformation during the heating process and shows an increasing trend with cold rolling reduction. The existence of retained austenite after cold rolling may promote the nucleation of the austenite and thus results in the increase of the activation energy with decreasing of austenite fraction.
(2) The apparent stored energy measured by DSC is mainly controlled by the phase transformation during the heating process. The maximum value of 30 J/g of the steel with 50%

thickness reduction is attributed to its lowest onset temperature. The onset temperature measured by DSC is found strongly dependent on the rolling strain and thus it is useful for the design of the heat treatment parameters of the annealing.

The DSC onset temperature of the cold rolled medium-Mn steel is chosen to be the annealing temperature, which results in a very good combination of strength and ductility. This result is very useful for the parameter design of batch annealing and continuous annealing of the cold rolled medium-Mn steel of the steel.

## Acknowledgment

The authors wish to thank the finial supports by the National Natural Science Foundation of China (Nos. 51371057 and 51101036) and National Basic Research Program of China (973 Program, No. 2010CB630803) and National Key Technology R&D Program (No. 2013BAE07B05).

## References

[1] S. Curtze, V.-T. Kuokkala, M. Hokka, et al., Mater. Sci. Eng. A 507 (2009) 124.
[2] A. Arlazarov, M. Goune, O. Bouaziz, et al., Mater. Sci. Eng. A 542 (2012) 31.
[3] R.A. Grange, C.R. Hribal, Edgar C. Bain, Lab. Fundam. Res., Rep. No.1453, USS, November 1968.
[4] R.L. Miller, R.A. Grange, Edgar C. Bain. Lab. Fundam. Res.. Rep. No. 1546.. USS, May 1970.
[5] R.L. Miller, Metall. Trans. 3 (1972) 905.
[6] W.Q. Cao, C. Wang, J. Shi, M.Q. Wang, W.J. Hui, H. Dong, Mater. Sci. Eng. A 528 (2011) 6661.
[7] M.B. Bever, Prog. Mater. Sci. 17 (1973) 5.
[8] G.W.H Höhne, W.F Hemminger, H.J. Flammersheim, Differential Scanning Calorimetry, Springer Verlag, Berlin, Heidelberg, New York, 2003.
[9] R.L. Danley, Therm. Acta 395 (2002) 201.
[10] C.Y. Wang, J. Shi, W.Q. Cao, H. Dong, Mater. Sci. Eng. A 527 (2010) 3442.
[11] W. Zhan, L.Q. Cao, J. Hu, W.Q. Cao, J. Li, H. Dong, J. Iron Steel. Res. Int. 21 (2014) 551.
[12] S.K. Nath, S. Ray, V.N.S. Mathur, M.L. Kapoor, ISIJ-Int. 34 (1994) 191.
[13] R.O. Rocha, T.M.F. Melo, E.V. Pereloma, D.B. Santos, Mater. Sci. Eng. A 391 (2005) 296.
[14] H.E. Kissinger, Anal. Chem. 11 (1957) 1702.
[15] F. Scholz, J.H. Driver, E. Woldt, Scr. Mater. 40 (1999) 949.
[16] E.A. Brandes, G.B. Brook (Eds.), Smithells Metals Reference Book (7th Ed.) Butterworth-Heinemann Ltd, Oxford, UK (1992).
[17] T. Taoka, K. Suzuki, A. Yoshikawa, M. Okamoto, Acta. Metall. 13 (1965) 1311.
[18] F. Scholz, E. Woldt, J. Therm. Anal. Calorim. 64 (2001) 895.
[19] Sujoy S. Hazra, Azdiar A. Gazder, Elena V. Pereloma, Mater. Sci. Eng. A 524 (2009) 158.
[20] W.Q. Cao, C. Wang, C.Y. Wang, J. Shi, M.Q Wang, H. Dong, Y.Q. Weng, Sci. China – Technol. Sci. 55 (2012) 1814.